Molecular Catalysis 468 (2019) 117–124

Contents lists available at ScienceDirect

Molecular Catalysis

journal homepage: www.elsevier.com/locate/mcat

Effect of zirconia polymorph on the synthesis of diphenyl carbonate over supported lead catalysts

Songlin Wang[a,b], Hongying Niu[a], Mengjun Guo[a], Jianji Wang[b], Tong Chen[c,*], Gongying Wang[c]

[a] School of Chemistry and Chemical Engineering, Henan Institute of Science and Technology, Xinxiang 453003, China
[b] Postdoctoral Programs, Key Laboratory of Green Chemical Media and Reactions, Ministry of Education, School of Chemistry and Chemical Engineering, Henan Normal University, Xinxiang 453007, China
[c] Chengdu Institute of Organic Chemistry, Chinese Academy of Sciences, Chengdu 610041, China

ARTICLE INFO

Keywords:
Diphenyl carbonate
Dimethyl carbonate
Tetragonal zirconia
Monoclinic zirconia

ABSTRACT

Zirconia supported Pb-based catalysts with purely tetragonal/monoclinic crystals were prepared and analyzed well by XRD, TEM-EDS, XPS, H_2-TPR, BET, Py-IR and NH_3-TPD techniques. The results indicate that zirconia polymorph has great effect on their structure and catalytic property for the synthesis of diphenyl carbonate (DPC) through methyl phenyl carbonate (MPC) disproportionation due to the differences of surface chemical properties, and tetragonal zirconia supported lead catalyst (TZ-Pb) shows bigger dispersion degree of PbO, higher surface area and Lewis acid amounts and thereby exhibits higher catalytic activity and selectivity compared to monoclinic zirconia supported catalyst (MZ-Pb). Furthermore, TZ-Pb shows better reusability due to strong metal-support interaction and may be readily recycled for at least four times without remarkable reactivity loss. This work provides a prospective reference for the facile and efficient synthesis of zirconia polymorph materials in various catalysis applications.

1. Introduction

Polycarbonate (PC) is significant engineering thermoplastic resin and has been widely utilized in chemical industry because of its superior electrical, heat resistance, and mechanical properties [1,2]. Diphenyl carbonate (DPC) is the main raw feedstock for the production of PC and is also a crucial chemical intermediate in the synthesis of fine chemicals, polymer materials, pharmaceuticals and other fields [3,4]. So far several alternative technologies for the preparation of DPC have been developed in the industry, and the transformation between phenol and dimethyl carbonate (DMC) into DPC is regarded as a best alternative approach to avoid toxic phosgene as starting material, which subsequently reacts with bisphenol-A to produce PC [5–9]. However, due to severe thermodynamic constraint concerning the transesterification from phenol and DMC ($K_P = 3.0 \times 10^{-4}$, 180 °C), the production of DPC is highly unfavorable even at high temperatures, and thereby numerous studies have focused on the process. The reaction starts from the transesterification of phenol and DMC to methyl phenyl carbonate (MPC) and methanol (Scheme 1-1), followed by MPC disproportionation to DPC and DMC (Scheme 1-2), or MPC continues to react with phenol to produce DPC and methanol (Scheme 1-3), but from K_2 (0.19, 25 °C) and K_3 (1.2×10^{-5}, 25 °C), DPC is mainly generated by the disproportionation. As both K_1 and K_2 are much small, the key of the process is the development of efficient catalytic system. Besides, in comparison with the two step reactions regarding Eq. (1) and Eq. (2), the first step is the rate-determining step, thus most studies to date have extensively focused on the first-step reaction [10–14]. Nevertheless, only little work has been made regarding the second-step disproportionation [15,16], moreover, in previously published work the disproportionation can hardly carry out thoroughly and restrict greatly the production of DPC [10–14]. Thus, considering the disproportionation reaction is the key step to the production of DPC, it is very valuable to further study on this reaction.

The conversion of MPC to DPC is extremely low because the reaction is kinetically and thermodynamically unfavorable. Thus, it is significantly demanded for developing new and efficient catalysts with high reactivity and stability. Several catalytic formulations have been explored for MPC disproportionation, mostly based on organo-titanium/tin, metal oxides and supported metal oxide catalysts [16–18]. Because of the difficulty of separation and recovery between the product and catalyst for homogeneous organo-titanium/tin as well as the low catalytic activities of metal oxides, much more attention has been now paid on supported metal-oxide catalysts, by contrast, zirconia supported lead is found to exhibit better catalytic properties than others

---

* Corresponding author.
E-mail address: chentongw@sina.com.cn (T. Chen).

https://doi.org/10.1016/j.mcat.2019.02.021
Received 31 October 2018; Received in revised form 9 February 2019; Accepted 22 February 2019

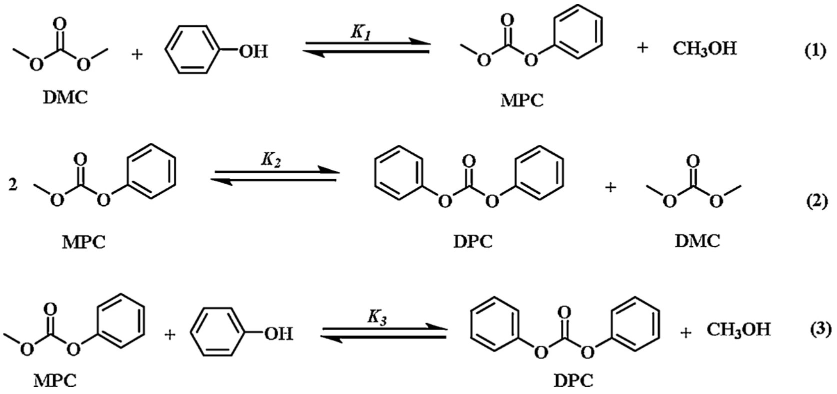

Scheme 1. Transesterification process between DMC and phenol into DPC.

for the disproportionation [18,19]. Nevertheless, it is well known that zirconia exhibits various crystals such as tetragonal, monoclinic and cubic crystal structures, where the coordination state of oxygen and zirconium are different due to different surface chemical properties. In the monoclinic crystal, O^{2-} is tricoordinated/tetracoordinated and Zr^{4+} is heptacoordinated, however, in the tetragonal crystal, O^{2-} is tetracoordinated and Zr^{4+} is octacoordinated [20,21]. The differences of zirconia crystalline phase as supports, especially for metal oxide catalysts, have usually significant influence on the dispersion, structure and nature of active component as well as the interaction strength and so on [22,23]. For example, several studies have reported that monoclinic/tetragonal zirconia as catalysts or supports show distinctly different catalytic activities in lots of reactions such as the direct synthesis of HBP from CO_2 and phenol, the glycerol dehydration to acrolein, the CO hydrogenation to synthesize methanol, the *n*-butane isomerization and so on [24–27].

Considering that zirconia possesses notable physical-chemical properties and displays good catalytic properties that are also remarkably influenced by crystal phase, the employment of different zirconia phase is important for many materials or catalytic reactions. To the best of our knowledge, there is no report about the effect of zirconia polymorph on the structure-catalytic properties relationship of Pb-based catalysts for MPC disproportionation. Thus, in the current work, in order to understand the effect of zirconia crystallite phase on its structure and catalytic property for MPC disproportionation, tetragonal and monoclinic zirconia supported Pb-based catalysts were prepared and characterized by transmission electron microscope (TEM), X-ray photoelectron spectroscopy (XPS), X-ray powder diffraction (XRD), temperature programmed reduction of H_2 (H_2-TPR), pyridine-infrared spectroscopy (Py-IR), N_2 adsorption/desorption and temperature programmed desorption of NH_3 (NH_3-TPD), as well as that the stability of the catalysts was also investigated in detail.

2. Experimental section

2.1. Material preparation

All reagents were supplied by Sigma-Aldrich Chemical Reagent Company, which were used as received without further purification.

According to a modified literature procedure [28,29], zirconium hydroxide was prepared by precipitation process. $ZrOCl_2{\cdot}8H_2O$ was dissolved into the water and slowly heated to 90 °C to form an aqueous solution. Ammonia solution with 25% concentration was added into this solution under stirring until that the pH of 9.3 was reached. After the precipitation completed, the solid sediment was aged at 60 °C overnight. Subsequently, the obtained mixture was vacuum filtered off, and the filter cake was washed repeatedly until no Cl^- was detected by using $AgNO_3$ solution (20 mg/L) in the filtrate and then dried at 100 °C to obtain zirconium hydroxide. Finally, tetragonal and monoclinic zirconia was prepared by calcination of as-prepared zirconium hydroxide at 500 and 750 °C for 5 h. The obtained sample was denoted as TZ and MZ, respectively.

TZ and MZ supported lead catalysts were prepared using incipient wetness impregnation process. The corresponding sample was impregnated with required amount of $Pb(NO_3)_2$ aqueous solution and kept for 24 h at room temperature. Afterwards, they were dried, and then calcinated for 5 h at 500 °C. The as-synthesized catalyst was designated as TZ-Pb and MZ-Pb, respectively. The PbO loading amount was 13 wt %.

2.2. Material characterization

X-ray diffraction pattern was recorded using X'pert DX-2700B diffractometer (Philip) with Ni-filtered Cu Kα radiation source (0.15418 nm). The sample was scanned in 2θ range of 0 to 90° with a scanning rate of 0.02° /second at the operating voltage and current of 40 kV and 30 mA. The crystal phase was identified by comparison with reference patterns in the JCPDS database.

The textural properties of the catalysts were determined by nitrogen adsorption/desorption isotherms at −196 °C (3H-2000PS2, BeiShiDe Instrument). Specific surface area and pore size distribution were calculated by BET equation and BJH method, respectively. Prior to measurement, the sample was degassed at 250 °C for 6 h under vacuum to remove the physiosorbed moisture.

The composition of the catalysts was performed by X-ray fluorescence spectroscopy (EDX1800B). The energy resolution was 165 ± 5 eV, and the peaks of Pb and Zr were identified by analyzer crystal. Before the measurement, the curve was firstly calibrated by standard samples, and then the element content of the samples was carried out.

X-ray photoelectron spectroscopy (XPS) was measured on Kratos Model XSAM 800 spectrometer with an exciting X-rays source of Al Kα = 1486.6 eV. The C1 s line at 284.6 eV was used for the correction of binding energies.

Transmission electron microscopic photograph (TEM) was carried out on TECNAIG2F20-S-TWIN electron microscope with 200 kV accelerating voltage, and the elemental maps were recorded by the energy dispersive spectrometer (EDS). The sample was prepared by grinding the powder, and then dispersed into an ethanol solution followed by ultrasonication. Then one droplet of the suspension was placed on carbon-coated copper grid, and finally evaporated for measurement.

The metallic Pb dispersion was determined by hydro-oxygen titration pulse method on Micro TP-5080 chemisorption analyzer. First, sample was pretreated at 400 °C for 1 h, and then the temperature was lowered to 120 °C in flowing H_2 atmosphere. Afterwards, the gas was switched to flowing N_2 (20 mL/min) and flushed for 3 h, followed by saturating with flowing O_2 at 120 °C for 30 min. Finally, the baseline was stabilized in flowing N_2, and then H_2 was introduced into the N_2

flowing by means of the calibrated sample to titrate the O_2. The amount of chemisorbed H_2 was obtained by subtracting the two isotherms, and the dispersion was calculated by assuming H_2 dissociative adsorption on the Pb metallic atoms.

Temperature-programmed reduction of H_2 (H_2-TPR) was performed using Micro TP-5076 chemisorption analyzer. Typically, catalyst was first flushed with flowing N_2 of 20 mL/min for 50 min at 400 °C and then cooled to room temperature. Subsequently, the temperature was heated up to 800 °C in flowing hydrogen-nitrogen mixture (containing 10 vol.% of hydrogen) at a heating rate of 10 °C/min, and the consumption H_2 was monitored with thermal conductivity detector. The quantification of H_2 was calculated by a calibration curve of CuO as standard.

Ammonia temperature programmed desorption (NH_3-TPD) was conducted by the same instrument as that used for H_2-TPR. Before adsorption, the catalyst was first pretreated at 400 °C for 1.5 h under N_2 flow. When the temperature cooled down to ambient temperature, NH_3 was performed by a flowing stream of 12 mL/min for 40 min. Subsequently, N_2 flow was introduced to remove physically adsorbed ammonia, and then NH_3 desorption was taken up to 800 °C at a heating rate of 10 °C/min.

Pyridine-infrared spectroscopy (Py-IR) was carried out to detect the acidic property of the catalysts. Sample was pressed into disks and placed at a quartz cell, which was pretreated under vacuum for 3 h at 300 °C to evacuate adsorbed impurities. When the temperature cooled down to ambient temperature, the sample was exposed to pyridine for 1 h and then outgassed for 2 h to remove the physically adsorbed pyridine. Finally, FT-IR spectra were measured.

2.3. Catalytic performance evaluation

The disproportionation of MPC was conducted in three-necked round-bottom flask connected to a liquid dividing head at atmosphere pressure. Typically, under nitrogen atmosphere, 150 mmol MPC and catalyst was added into the flask. When the reaction was heated up to the desired temperature under stirring, the temperature was kept. During the reaction procedure, DMC distillate was collected in a receiver flask to break the equilibrium limitation towards the formation of DPC. After the reaction completion, the mixture was gradually cooled down to room temperature. The catalyst was filtered, and the products in the reaction mixture were detected by GC–MS analyses using HP-6890/5973 gas chromatograph equipped with HP-5 capillary column (30 m × 0.25 mm × 0.25 um). The conversion, yield and selectivity were quantitatively analyzed using GC-7890 A gas chromatograph with HP-5 capillary column (30 m × 0.32 mm × 0.25 μm) and FID detector.

3. Results and discussion

3.1. Material characterization

3.1.1. Structural and textural characterization

Fig. 1 displays XRD patterns of pure and zirconia supported Pb-based catalysts. When as-prepared zirconium hydroxide is calcined at 500 °C, the obtained TZ exhibits a purely tetragonal phase structure (2θ = 30.3, 35.2, 50.2 and 60.2°, JCPDS No. 27-997) [30,31]. The obtained MZ by calcination of 750 °C is predominantly monoclinic phase structure (2θ = 24.1, 28.3, 31.5, 34.2 and 50.4°, JCPDS No. 37-1484) and only a weak diffraction peak of tetragonal phase at 2θ = 30.3° is noticed. After lead addition, there is mostly the existence of tetragonal phase for TZ-Pb and two weak diffraction peaks assigned to monoclinic phase are observed at 28.3 and 31.5°, suggesting that the introduction of lead results in the structure transformation of tetragonal phase, while no diffraction peaks belonging to PbO crystalline phases are detected, which suggest that the lead dispersion on TZ-Pb catalyst is good, and lead oxide may be highly dispersed on the catalyst surface.

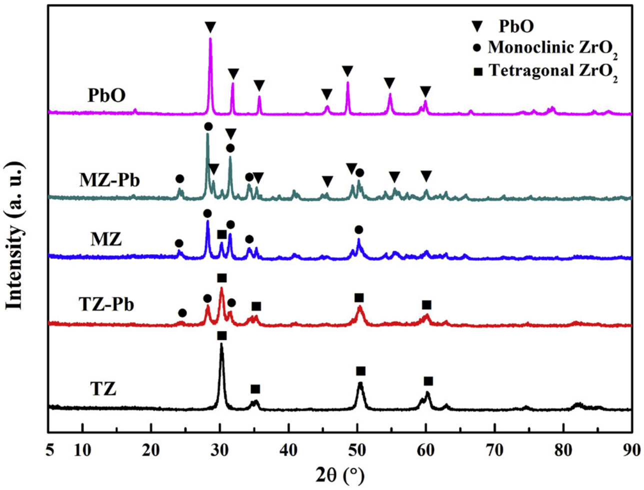

Fig. 1. XRD patterns of pure and zirconia supported Pb-based catalysts.

For MZ-Pb catalyst, monoclinic zirconia phases remain stable, but PbO crystalline phases appear at ca. 29.1, 31.5 35.4, 45.6, 49.3, 55.5 and 60.1° whose partial diffraction peaks overlap with those of MZ, and this reason is probably due to the different support properties of zirconia polymorphs. Thus, it may be inferred that the introduction of lead has a great influence on the crystalline organization of zirconia. The XRD results indicate that the dispersion of PbO on TZ-Pb is higher than MZ-Pb. For further confirmation, the lead dispersion degree is also determined by hydro-oxygen titration and the result is listed in Table 1. Clearly, TZ-Pb exhibits a higher dispersion degree than that of MZ-Pb, which was consistent with the XRD analysis.

The textural properties of all the samples determined by nitrogen adsorption/desorption are listed in Table 1, and they exhibit great difference in surface area, pore volume and pore size. The surface area and pore volume of TZ-Pb remarkably decrease as comparison with those of pure TZ support, but the pore size is almost unchanged, which may be ascribed to the dispersion and deposition of PbO on the surface of TZ. However, for MZ-Pb catalyst the surface area and pore volume show nearly no change as comparison with MZ. It probably suggests that PbO is not evenly distributed on MZ support due to relatively small surface area, resulting in the low dispersion. Moreover, the surface composition of TZ-Pb and MZ-Pb is determined by XRF technique, and Table 1 displayed that the surface molar ratio of Pb to Zr over MZ-Pb is larger than the nominal molar ratio of 0.082, further suggesting the aggregation of PbO on MZ support, and it is well in line with the characteristic peaks of PbO observed in the XRD patterns. Consequently, the structural and textural differences for TZ-Pb and MZ-Pb are distinctly associated with the different support properties of zirconia polymorphs. In contrast, TZ-Pb reveals not only the higher dispersion of PbO but also larger BET surface areas, and therefore it is favorable to expose more active sites, contributing to the improvement of its

Table 1
The textural properties of pure and zirconia supported Pb-based catalysts.

Catalysts	S_{BET} (m^2/g)	Pore volume (cm^3/g)	Average pore diameter (nm)	Pb/Zr[a]	Pb/Zr[b]	Pb dispersion[c]
TZ	43	0.127	7.0	–	–	–
TZ-Pb	34	0.099	7.0	0.082	0.091	0.016
MZ	15	0.126	20.0	–	–	–
MZ-Pb	13	0.101	20.0	0.082	0.103	0.007

[a] Calculated by Pb and Zr stoichiometric molar ratio.
[b] Measured by XRF.
[c] Determined by hydro-oxygen titration method.

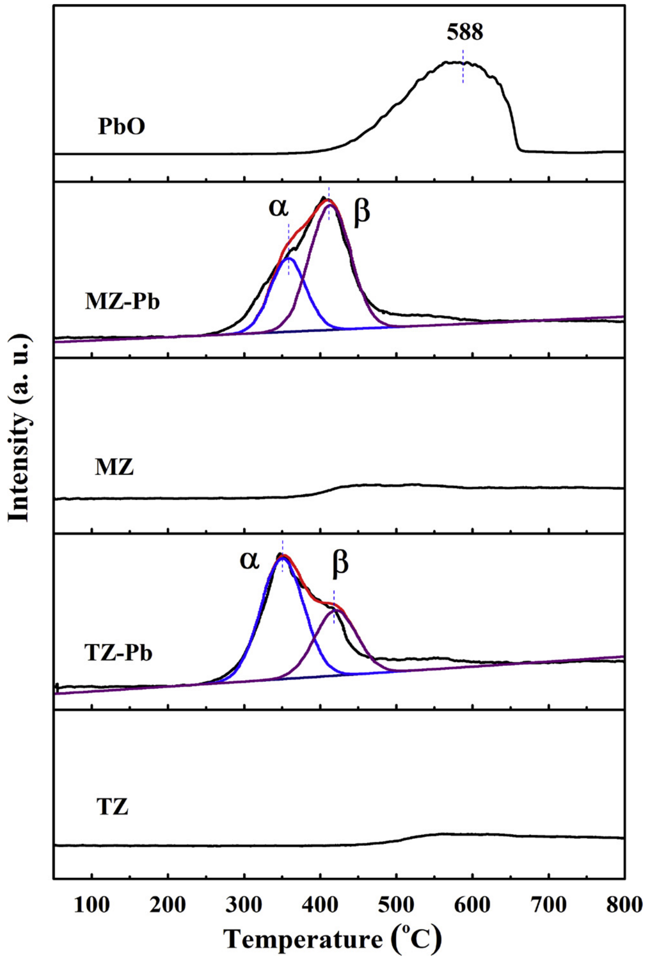

Fig. 2. H_2-TPR profiles of pure and zirconia supported Pb-based catalysts.

catalytic ability.

3.1.2. H_2-TPR characterization

Fig. 2 displays the H_2-TPR profiles of pure and zirconia supported Pb-based catalysts. PbO shows a broad hydrogen consumption peak at 588 °C, which is assigned to PbO species reduction. Both pure TZ and MZ present very weak hydrogen reduction peaks at the range from 450 to 600 °C that can hardly be observed, while TZ-Pb exhibits a broad but well-defined peak in the range of 250–500 °C, therefore mainly PbO is reduced. Likewise, MZ-Pb has a similar reduction pattern. For a clear observation, they are integrated by Gaussian function fitting to calculate their respective amounts in Table 2, respectively. Two peaks can be observed at 350 °C (referred to as peak α) and 417 °C (peak β) for TZ-Pb catalyst, corresponding to the highly dispersed lead species and bulk lead oxide reduction [14,26]. And the hydrogen consumption of α peak is approximately twice higher than that of β peak. Similar to that of TZ-Pb, MZ-Pb shows also two reduction peaks at 358 °C (peak α) and 411 °C (peak β), but the hydrogen consumption of peak α is twice lower than that of peak β. Generally, such low reduction temperature range and high hydrogen consumption of peak α (as compared to peak β) usually corresponds to high metal dispersed phase with small crystallite size and the large interaction with support [32,33], which is in agreement with the below TEM and XPS analysis. In contrast, TZ-Pb exhibits the lower reduction temperature and larger hydrogen consumption of α peak, and thus it possesses a stronger interaction between lead and zirconia support, which would be favorable for improving the catalyst stability during reaction. The results further testify that the difference of reduction performance for TZ-Pb and MZ-Pb is largely dependent on the surface property of zirconia support, which has great influence on the surface nature of lead oxide and the interaction with zirconia.

Table 2
The reduction performances of TZ-Pb and MZ-Pb determined by H_2-TPR.

Catalysts	Reduction temperature (°C)		H_2 consumption (mmol/g)		Total consumption (mmol/g)
	peak α	peak β	peak α	peak β	
TZ-Pb	350	417	0.074	0.040	0.114
MZ-Pb	358	411	0.042	0.084	0.126

3.1.3. TEM characterization

Fig. 3 presents the TEM pictures of TZ-Pb and MZ-Pb, and their elemental distribution mapping images are also given. As shown in Fig. 3, the catalysts show different morphological structures. TZ-Pb in Fig. 3(A, B) mainly exhibits round-sheet-like morphological structures with uniform and homogeneous particles, and most of them seem to have smaller particle size (˜18 nm). While for MZ-Pb in Fig. 3(C, D), it can be seen that MZ-Pb with larger particle size (˜45 nm) represents flake-like crystals, which is remarkably different from TZ-Pb. The catalytic activity is related to particle size, and a small size is beneficial to the disproportionation of MPC. TZ-Pb has a small diameter with good PbO dispersion, which is conducive to improving the catalytic activity of the catalyst. The EDS spectrum further confirms the existence of Pb on the surface of the supports (Fig. S1, Supplementary Information), which evidently indicates that the Pb element is highly dispersed on the surface of TZ-Pb in comparison with MZ-Pb, and this is also consist with the result of XRD characterization.

3.1.4. XPS characterization

XPS spectra of the catalysts are conducted to further investigate the element nature, and the results are revealed in Fig. 4. Fig. 4(A) displays the deconvolution of Zr 3d of the catalysts, and TZ and MZ exhibit clearly two characteristic peaks at around 181.8 and 184.2 eV, which are attributed to Zr $3d_{5/2}$ and Zr $3d_{3/2}$ consecutively, which is in accordance with the literature reports [34,35], suggesting that only Zr^{4+} exists in the pure supports. Apparently, for TZ-Pb and MZ-Pb, the binding energies are shifted towards higher values when the lead is added, suggesting the formation of Pb − O − Zr bonds. Fig. 4(B) displays the deconvolution of Pb 4f in TZ-Pb and MZ-Pb, the binding energies centered at around 138.7 and 143.5 eV are observed, corresponding to Pb $4f_{7/2}$ and Pb $4f_{5/2}$, respectively. According to literature [36], the binding energy of Pb $4f_{7/2}$ and Pb $4f_{5/2}$ in PbO is 137.0 and 142.0 eV, and evidently the binding energies in TZ-Pb and MZ-Pb are also shifted to higher values upon the Pb − O − Zr formation. Fig. 4(C) displays the deconvolution of O 1 s of the catalysts, and two characteristic peaks located at around 530.0 and 531.2 eV are exhibited in TZ and MZ, which are ascribed to lattice oxygen of metal-oxides (such as O^{2-}) and adsorbed oxygen species (such as O- and O^{2-}) on the surface [37,38], respectively. Nevertheless, after the addition of lead, the binding energies in TZ-Pb and MZ-Pb are shifted to the lower values. Based on these results, the reasons for the binding energy changes of Zr, Pb and O in TZ-Pb and MZ-Pb can likely be accounted for electron density variation due to the Pb − O − Zr formation, resulted in the electron from Zr and Pb flowing to O because of higher electronegativity of O compared to Zr and Pb, indicating that there is an interaction between lead and zirconia. In comparison, TZ-Pb exhibits the larger binding energy variations, suggesting a stronger interaction between lead and zirconia support, which is in good conformity with H_2-TPR analysis.

3.1.5. NH_3-TPD characterization

NH_3-TPD measurements are conducted to study the acid properties, and the acid strength and acidity of the catalysts can be evaluated according to their typical desorption peak. Fig. 5 displays the NH_3-TPD

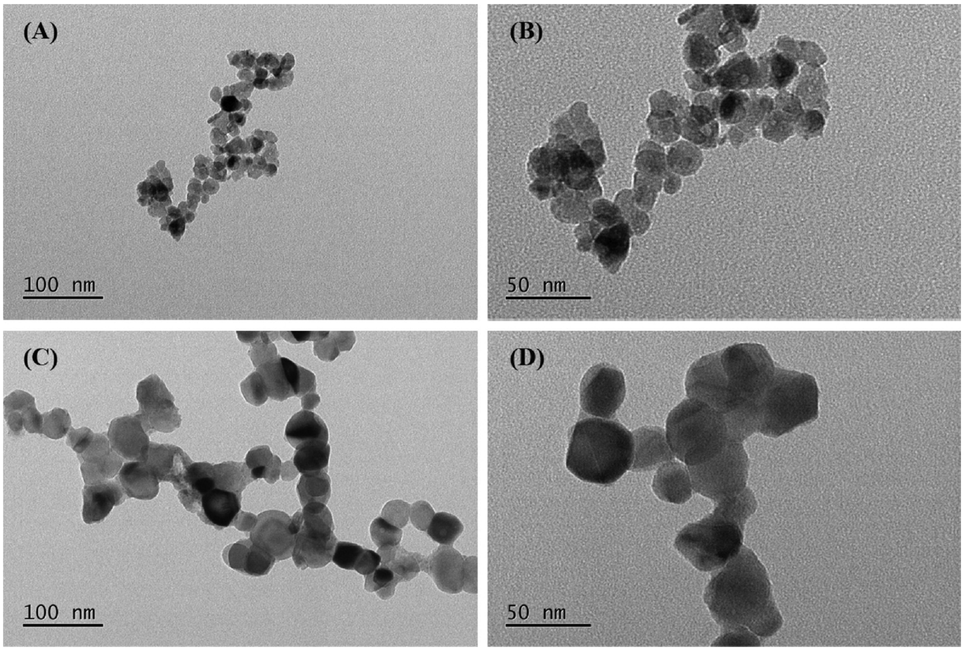

Fig. 3. TEM pictures of zirconia supported Pb-based catalysts: TZ-Pb (A, B) and MZ-Pb (C, D).

profiles of pure and zirconia supported Pb-based catalysts. There are two notable NH_3 desorption peaks, and the peak at low temperature of around 160–490 °C represents weak acid site and the other at high temperature in the range of around 500–750 °C represents strong acid site [37,39], respectively. The areas of desorption peaks are linearly proportional to the acid amount. For a clear comparison, the profiles are deconvoluted by Gaussian function fitting, and the acid amount is quantitatively calculated from the peak areas in Table 3. It can be seen that this crystalline structure remarkably influences the acidity, and TZ has higher surface acid amount than MZ. Interestingly, after introducing lead into TZ and MZ, the acid amounts of both TZ-Pb and MZ-Pb decrease. The reasons are probably that PbO possesses both Lewis acidic and basic properties, and lead could be easily combined or coordinated with Zr by Lewis acid-base interactions through Zr–O–Pb bond, resulted in the decrease of acid amount. Moreover, the larger surface acid amount of TZ than MZ suggests that it can be more readily interacted with Pb species after impregnating, thereby causing the higher dispersion of PbO as well as forming the stronger interaction between lead and TZ support, this analysis is in good accordance with the above discussion of XRD, H_2-TPR and XPS results. Although the acid amounts decrease, the total acid amount in the TZ-Pb is remarkably higher than that of the MZ-Pb catalyst, which is conductive to adsorb and activate MPC molecules, improving the catalytic activity.

3.1.6. Py-IR characterization

To obtain the information of Brønsted and Lewis acidity, the pyridine-infrared spectroscopy of the catalysts is detected. Fig. 6 displays the Py-IR spectra of zirconia supported Pb-based catalysts, and the concentration ratio of Brønsted to Lewis acidity is given in Table 3. The infrared absorptions at 1590 and 1440 cm^{-1} are assigned to pyridine bound interacting with Brønsted and Lewis acid sites, respectively [34,40,41]. TZ displays a remarkable absorption peak at 1440 cm^{-1} and a weak absorption peak at 1590 cm^{-1}, while MZ exhibits two obvious absorptions peak, indicating that TZ possesses mainly the presence of Lewis acidic sites, and MZ contains both Brønsted and Lewis acid sites, which is in line with literature reported previously [21]. By the addition of lead, the acidic centers do not change remarkably for MZ-Pb, whereas for TZ-Pb they are affected that the peak intensities increase obviously, leading to an increased acidity on the surface. As can be seen in Table 3, the ratios of B/L for TZ and TZ-Pb are lower than those of MZ and MZ-Pb. As a result, the results of Py-IR and NH_3-TPD suggest that TZ and TZ-Pb own much higher Lewis acidity, contributing to MPC disproportionation because this reaction was Lewis acid catalysis process.

3.2. Results of the catalytic evaluation for MPC disproportionation

Fig. 7 displays the results of MPC disproportionation over the catalysts. This crystalline form strongly influences the catalytic activity of Pb-based catalysts. Pure TZ and MZ supports are found to be weak catalytic activities under the present experimental conditions, and the introduction of lead after impregnating shows noticeable improved catalytic activities, implying that lead is the active component phases while TZ and MZ mainly act as the catalyst supports although they possess larger BET surface area and higher acid amount compared to supported Pb-based catalysts. For TZ-Pb and MZ-Pb, the MPC conversion and DPC selectivity are 65.1%, 99.1% and 48.8%, 98.4% respectively, indicating that TZ-Pb exhibits better catalytic performance. Moreover, the TON value of TZ-Pb reaches up to 140 mol MPC/mol Pb for MPC conversion obtained at 50 min, which is also obviously higher than 103 mol MPC/mol Pb of MZ-Pb. The results suggest that the TZ-Pb catalyst is more active than MZ-Pb, and thereby tetragonal zirconia is more suitable crystalline phase structure for MPC disproportionation compared to the monoclinic one.

In view of the characteristic results of Py-IR and NH_3-TPD, the catalytic activities for pure TZ and MZ supports are probably resulted from the presence of the acidic sites on its surface. Moreover, TZ reveals relatively higher catalytic activity compared to MZ because TZ has more numbers of Lewis acid sites. As the studies in previous work [18], the surface area and interaction of Pb and Zr play key role in the catalytic activity for supported lead catalysts. Thus, from the above characterized analysis results, TZ-Pb owns higher dispersion of PbO and larger surface area, which is very advantageous to resulting in more exposure of Lewis acid active sites to accessibly adsorb and activate MPC, thereby behaving better catalytic activity.

3.3. Recycling of the catalyst

The recycling of catalyst is a significant requirement for practical application. Therefore, the recyclability of the catalyst is examined, and

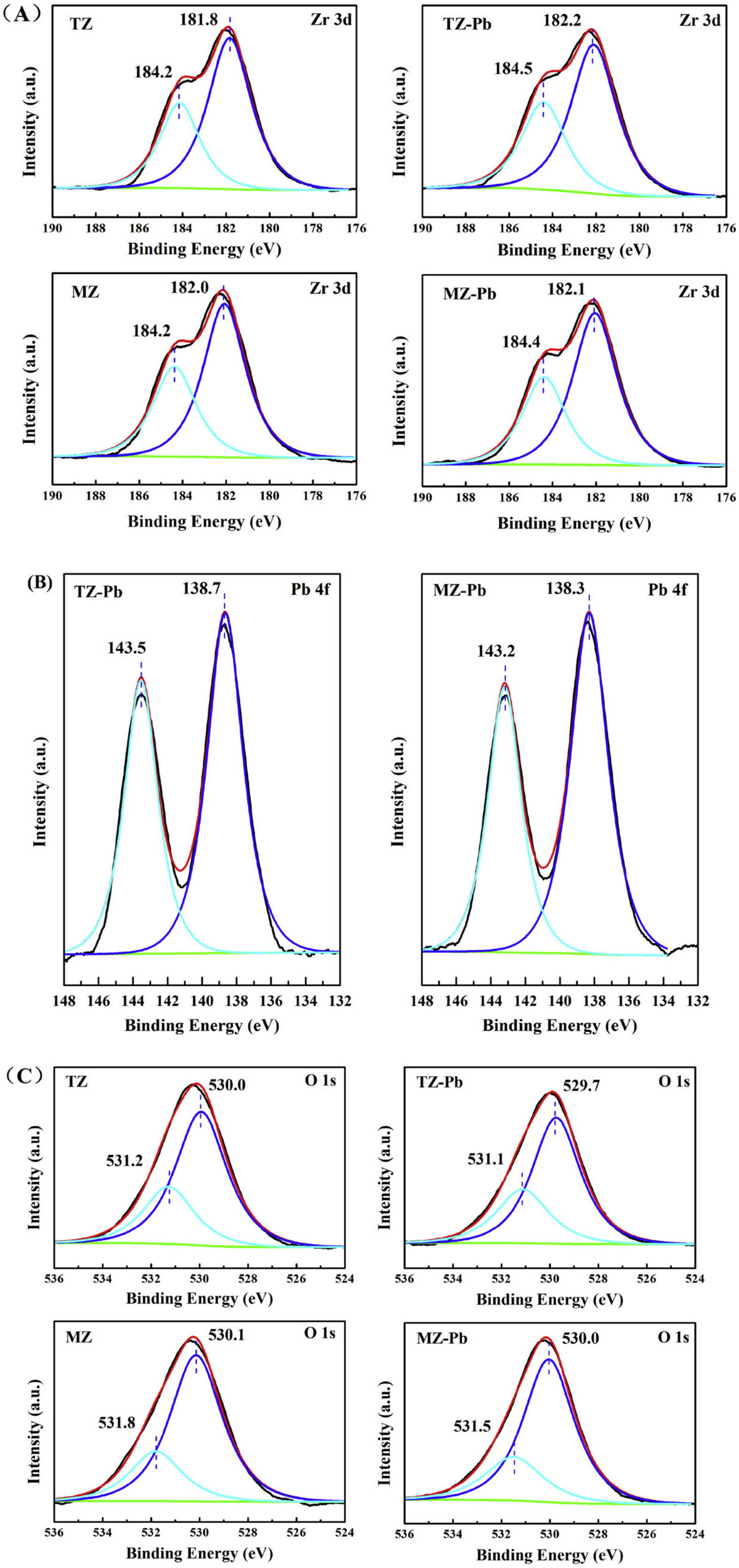

Fig. 4. XPS spectra of pure and zirconia supported Pb-based catalysts.

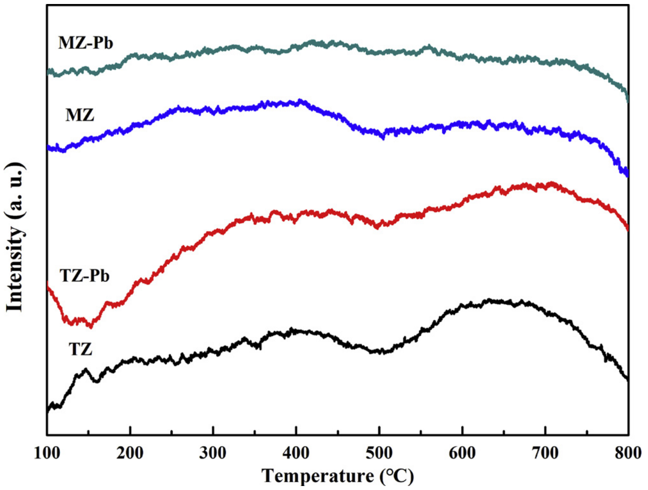

Fig. 5. NH_3-TPD profiles of pure and zirconia supported Pb-based catalysts.

Table 3
The acidity of pure and zirconia supported Pb-based catalysts determined by NH_3-TPD.

Catalysts	Acid strengths (°C)		Acid amounts (mmol/g)		Total acid amounts (mmol/g)	B/L ratio
	Weak	Strong	Weak	Strong		
TZ	394	671	0.054	0.114	0.168	0.410
TZ-Pb	346	707	0.068	0.047	0.115	0.983
MZ	404	716	0.056	0.040	0.096	1.166
MZ-Pb	421	725	0.019	0.034	0.053	1.104

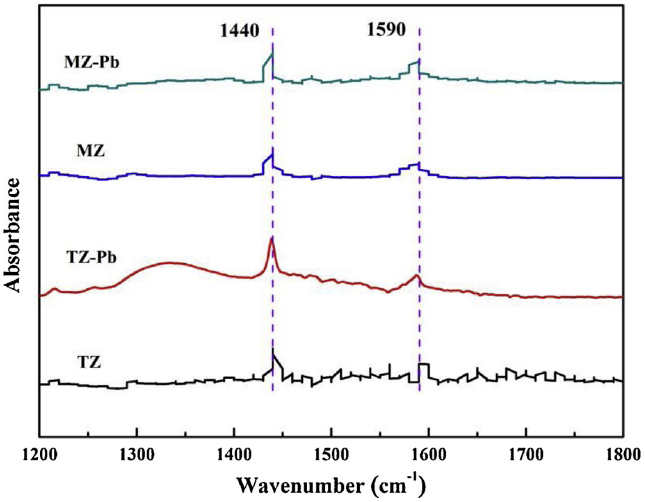

Fig. 6. Py-IR spectra of zirconia supported Pb-based catalysts.

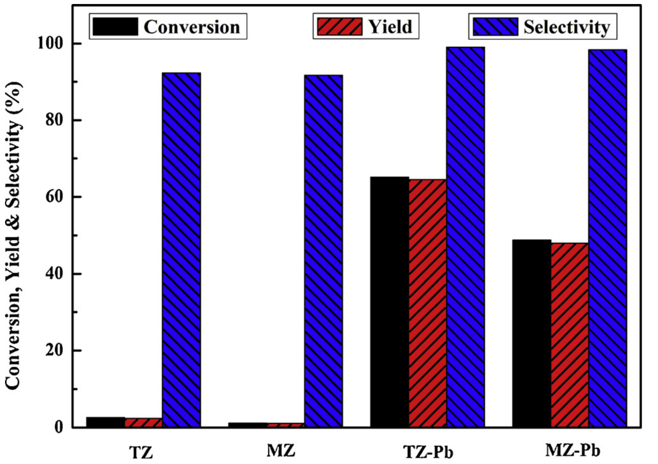

Fig. 7. Catalytic results of MPC disproportionation over the catalysts. Reaction conditions: catalyst 1.2 g, MPC 150 mmol, 200 °C, 2.5 h. Anisole is the trace by-product existence.

after each run completion the used catalyst is recovered by filtrating and washing with DMC, and then dried at 110 °C overnight. The results are illustrated in Fig. 8. The MPC conversion and DPC yield have no significant change over TZ-Pb in the four consecutive runs, nevertheless, for MZ-Pb, the catalytic activity decreases slightly from 48.8% to 43.5%, suggesting that TZ-Pb shows better stability compared to MZ-Pb. Elemental analysis of used TZ-Pb and MZ-Pb obtained by XRF presents that 0.8% and 1.5% Pb are leached out from fresh TZ-Pb and MZ-Pb after using four times, respectively, suggesting that TZ-Pb is more intact and there is little leaching loss of Pb during the reaction. Combining with the H_2-TPR and XPS analysis, the excellent recyclability of TZ-Pb is probably resulted from its stronger metal-support interaction.

Besides, TZ-Pb and MZ-Pb after the forth use are also detected by XRD in Fig. 9. The results show that the diffraction peak of used TZ-Pb and MZ-Pb is basically the same patterns as the respective freshly prepared catalysts, suggesting that no structural changes occur on the surface of the catalysts, and thereby tetragonal zirconia is more active and stable crystalline structure for MPC disproportionation.

4. Conclusions

In this paper, zirconia polymorph inflicts great difference on the structural properties of zirconia supported Pb-based catalysts. Moreover, the catalytic activities are also strongly influenced for the disproportionation of MPC, and tetragonal zirconia is more active and stable crystal phase compared to the monoclinic one. The conversion of MPC and yield of DPC reach 65.1% and 64.5% over TZ-Pb, which is significantly higher than that of MZ-Pb. And the TON value over TZ-Pb is also obviously higher than that of MZ-Pb. The characterization results indicate that the superior catalytic performance of TZ-Pb is related to its good dispersion degree of PbO, large specific surface area and high Lewis acidic active sites, which are relevant and together contribute to the improvement of catalytic activity. Additionally, TZ-Pb shows also better stability due to stronger metal-support interaction that after four consecutive runs there is no significant change in MPC conversion and DPC yield. Thus, this work has provided a prospective reference for the extensive utility of zirconia polymorph materials in broad catalysis areas.

Acknowledgments

This work was supported by the National High Technology Research and Development Program of China (863 program, No. 2013AA031703), the National Natural Science Foundation of China (No. 21808048), the Key Project of Science and Technology Program of Henan Province (182102210050), the Project funded by China Postdoctoral Science Foundation (2018M632782), the Science Research Start-up Fund of Henan Institute of Science and Technology (2015031), the Key Scientific Research Project of Colleges and Universities in Henan Province (17A150026), the Postdoctoral Start-up Fund of Henan Institute of Science and Technology, the Project funded by Postdoctoral Science Foundation of Henan Province, and the Project funded by Natural College Student Innovation and Entrepreneurship Training (S201810467007).

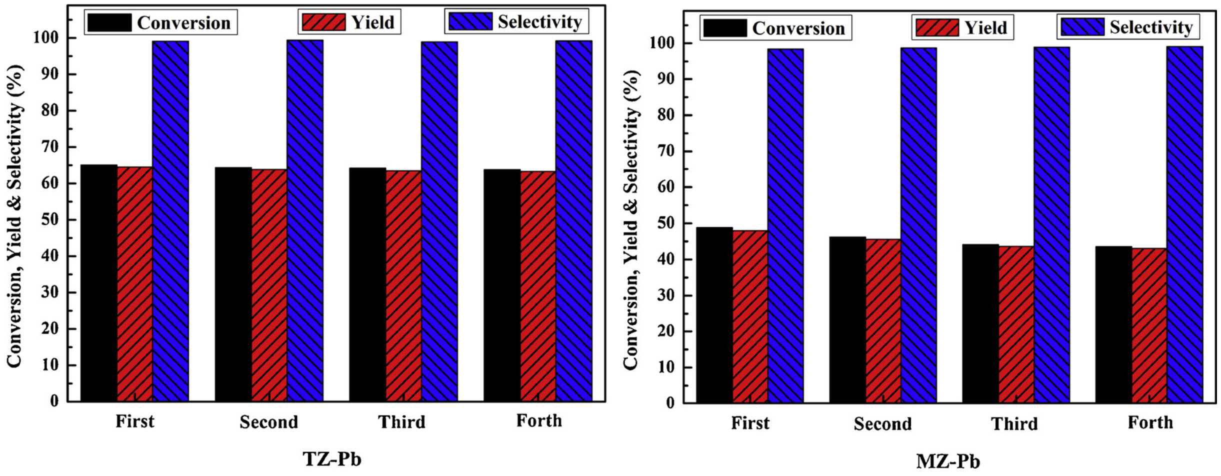

Fig. 8. Recycling of TZ-Pb and MZ-Pb for MPC disproportionation.

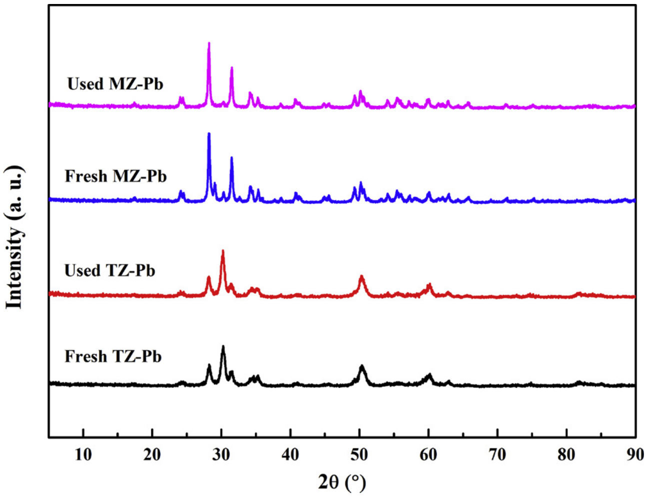

Fig. 9. XRD patterns of fresh and used catalysts after four times run.

Appendix A. Supplementary data

Supplementary material related to this article can be found, in the online version, at doi:https://doi.org/10.1016/j.mcat.2019.02.021.

References

[1] M.C. Figueiredo, V. Trieu, S. Eiden, J. Heijl, M.T.M. Koper, ACS Catal. 8 (2018) 3087–3090.
[2] E.R. Baral, J.H. Lee, J.G. Kim, J. Org. Chem. 83 (2018) 11768–11776.
[3] S. Bahrami, S.N. Khorasani, A. Abdolmaleki, S.M. Davoodi, A. Farzan, J. Elastom. Plast. 50 (2018) 107–123.
[4] G. Fiorani, A. Perosa, M. Selva, Green Chem. 20 (2018) 288–322.
[5] A. Gawdzik, A. Mederska, T. Mederski, Polym. Bull. 74 (2017) 1553–1571.
[6] G. Contreras-Zarazúa, J.A. Vázquez-Castillo, C. Ramírez-Márquez, G.A. Pontis, J.G. Segovia-Hernández, J.R. Alcántara-Ávila, Energy 165 (2017) 637–649.
[7] R. Kaneg, H. Ogihar, I. Yamanaka, Catal. Sci. Technol. 6 (2016) 6002–6010.
[8] S.H. Huang, B. Yan, S.P. Wang, X.B. Ma, Chem. Soc. Rev. 44 (2015) 3079–3116.
[9] G.Z. Fan, H.T. Zhao, Z.X. Duan, T. Fang, M.H. Wan, L.N. He, Catal. Sci. Technol. 1 (2011) 1138–1141.
[10] C.Z. Wang, T. Guo, M.M. Sun, C.H. Li, M. Guo, C.L. Li, Q. Wang, Sci. Adv. Mater. 10 (2018) 779–784.
[11] S. Han, M. Luo, X.L. Zhou, Z. He, L.P. Xiong, Ind. Eng. Chem. Res. 51 (2012) 5433–5437.
[12] Y.T. Kim, E.D. Park, Appl. Catal. A Gen. 356 (2009) 211–215.
[13] Y. Gao, Z.H. Li, K.M. Su, B.W. Cheng, Chem. Eng. J. 301 (2016) 12–18.
[14] W.Q. Zhou, X.Q. Zhao, Y.J. Wang, J.Y. Zhang, Appl. Catal. A Gen. 260 (2004) 19–24.
[15] W.B. Kim, J.S. Lee, J. Catal. 185 (1999) 307–313.
[16] S.L. Wang, Y.Z. Zhang, Y. Chen, R.Z. Tang, T. Chen, G.Y. Wang, Chem. J. Chinese U. 35 (2014) 2177–2181.
[17] W.B. Kim, Y.G. Kim, J.S. Lee, Appl. Catal. A Gen. 194/195 (2000) 403–414.
[18] S.L. Wang, C.G. Li, Z.L. Xiao, T. Chen, G.Y. Wang, J. Mol. Catal. A Chem. 420 (2016) 26–33.
[19] Q. Fu, Y.C. Ou, Y. Zeng, G.Y. Wang, Chem. Ind. Eng. Prog. (Chinese) 36 (2017) 2748–2755.
[20] K.H. Jacob, E. Knözinger, S. Benier, J. Mater. Chem. 3 (1993) 651–657.
[21] Y.B. Zhao, W. Li, M.H. Zhang, K.Y. Tao, Catal. Commun. 3 (2002) 239–245.
[22] A. Ulgen, W. Hoelderich, Catal. Lett. 131 (2009) 122–128.
[23] W. Stichert, F. Schüth, S. Kuba, H. Knözinger, J. Catal. 198 (2001) 277–285.
[24] Z.H. Li, K.M. Su, J. Mol. Catal. A Chem. 277 (2007) 180–184.
[25] S.R. Ginjupalli, S. Mugawar, N.P. Rajan, P.K. Balla, V.R.C. Komandur, Appl. Surf. Sci. 309 (2014) 153–159.
[26] Z.Y. Ma, C. Yang, W. Wei, W.H. Li, Y.H. Sun, J. Mol. Catal. A Chem. 231 (2005) 75–81.
[27] J.C. Yori, J.M. Parera, Catal. Lett. 65 (2000) 205–208.
[28] H.R. Mahmoud, J. Mol. Catal. A Chem. 392 (2014) 216–222.
[29] M. Wu, C.L. Li, J. Zhang, C.C. Miao, Y.P. Zheng, Y.M. Sun, Ind. Eng. Chem. Res. 51 (2012) 6304–6309.
[30] J.F.S. de Oliveira, D.P. Volanti, J.M.C. Bueno, A.P. Ferreira, Appl. Catal. A Gen. 558 (2018) 55–66.
[31] S.V.H.S. Bhaskaruni, S. Maddila, W.E. van Zyl, S.B. Jonnalagadda, Catal. Today 309 (2018) 276–281.
[32] S. Tada, K. Larmier, R. Buchel, C. Coperet, Catal. Sci. Technol. 8 (2018) 2056–2060.
[33] X.L. Zhang, D.F. Wang, G.D. Wu, X.L. Wang, X.X. Jiang, S.S. Liu, D.G. Zhou, D.M. Xu, J. Gao, Appl. Catal. A Gen. 555 (2018) 130–137.
[34] S. Pyen, E. Hong, M. Shin, Y.W. Suh, C.H. Shin, Mol. Catal. 448 (2018) 71–77.
[35] H.T. Wu, Y. Yang, H.Y. Suo, M. Qing, L. Yan, B.S. Wu, J. Xu, H.W. Xiang, Y.W. Li, J. Mol. Catal. A Chem. 396 (2015) 108–119.
[36] Z.H. Li, Y.J. Wang, X.S. Ding, X.Q. Zhao, J. Nat. Gas Chem. 18 (2009) 104–109.
[37] B.H. Jia, J.X. Guo, H.D. Luo, S. Shu, N.J. Fang, J.J. Li, Appl. Catal. A Gen. 553 (2018) 82–90.
[38] X.Y. Zhang, X.X. Cheng, C.Y. Ma, Z.Q. Wang, Catal. Sci. Technol. 8 (2018) 3336–3345.
[39] D.F. Wang, X.L. Zhang, X.S. Cong, S.F. Liu, D.G. Zhou, Appl. Catal. A Gen. 555 (2018) 36–46.
[40] W. Hertl, Langmuir 5 (1989) 96–100.
[41] M. Massa, A. Andersson, E. Finocchio, G. Busca, F. Lenrick, L.R. Wallenberg, J. Catal. 297 (2013) 93–109.